

Ferroelectricity induced by acentric spin-density waves in YMn_2O_5

L.C. Chapon,¹ P.G. Radaelli,^{1,2} G.R. Blake,^{1,3} S. Park,⁴ and S-W. Cheong⁴

¹*ISIS facility, Rutherford Appleton Laboratory-CCLRC,
Chilton, Didcot, Oxfordshire, OX11 0QX, United Kingdom.*

²*Dept. of Physics and Astronomy,
University College London, Gower Street,
London WC1E 6BT, United Kingdom*

³*Materials Science Division, Argonne National Laboratory, Argonne, Illinois 60439, USA*

⁴*Department of Physics and Astronomy,
Rutgers University, Piscataway, New Jersey 08854, USA*

(Dated: November 20, 2018)

Abstract

The commensurate and incommensurate magnetic structures of the magnetoelectric system YMn_2O_5 , as determined from neutron diffraction, were found to be spin-density waves lacking a global center of symmetry. We propose a model, based on a simple magneto-elastic coupling to the lattice, which enables us to predict the polarization based entirely on the observed magnetic structure. Our data accurately reproduce the temperature-dependence of the spontaneous polarization, in particular its sign reversal at the commensurate-incommensurate transition.

PACS numbers: 25.40.Dn, 75.25.+z, 77.80.-e

There is currently great interest in understanding the microscopic nature of the coupling between ferroelectricity and magnetic ordering in several transition metal oxides, such as RMnO_3 and RMn_2O_5 (R =rare earth element)[1, 2, 3, 4, 5, 6]. This coupling is responsible for the sensitivity of these materials to an applied magnetic field and may lead to new classes of functional materials. Unlike more conventional multiferroics such as BiFeO_3 and BiMnO_3 , the paramagnetic phase in these new materials is centrosymmetric, and electrical polarization appears only at the transition to a magnetically ordered phase. This implies that the ordered spin structure is responsible for removing the center of symmetry and generating a polar field. Two approaches have so far been proposed in the literature: the magneto-elastic effect could occur through a *scalar* field of the type $S_n \cdot S_{n+1}$, which must be coupled to a pre-existing polar field from the crystal structure, or through a *vector* field of the type $S_n \times S_{n+1}$ [6, 7, 8]. In the latter case, non-collinearity is a key ingredient to promote a polar state, whereas in the former case a collinear phase could in principle support electrical polarization. Naturally, in both cases, global inversion symmetry must be lost.

Recently we showed that, for TbMn_2O_5 [3], the largest electric polarization is associated with a commensurate magnetic (CM) state that is almost collinear. The magnetic structure can be described as a superposition of several amplitude-modulated waves on inequivalent lattice sites with non-coincident nodal points, making it acentric (the structure has constant moments for an appropriate choice of the global phase). On further cooling below 25 K, the TbMn_2O_5 magnetic structure becomes incommensurate (ICM) with $\mathbf{k} \sim (0.48, 0, 0.32)$. Although the electrical polarization evolves in a complex way through this transition, the ICM phase remains ferroelectric, displaying, at low temperatures, a remarkably strong coupling with an applied magnetic field[2]. It is therefore of great interest to solve the ICM structure and determine how global inversion symmetry is lost, since in a simple spin density wave (SDW) one can always find a lattice point that is also an inversion center. On the basis of theoretical considerations and experimental data, Kenzelmann and coworkers[5] propose that in TbMnO_3 inversion symmetry is broken by the development of a cycloidal magnetic structure, which can be described as a superposition in quadrature of two waves associated with different components of the magnetic moment on the *same* site. Here, we propose a different and, to our knowledge, hitherto unexplored mechanism for the ICM phases of the RMn_2O_5 series: the loss of inversion symmetry arises from the superposition of two waves on *different* crystallographic sites, each with an independent phase factor. In the specific case

of YMn_2O_5 , where we have solved both CM and ICM structures from neutron diffraction data, we show that the temperature dependence of the electrical polarization as calculated from the magnetic structure using a simple $S_n \cdot S_{n+1}$ exchange coupling is consistent with the measurement of electrical properties[9]. In particular, our model is capable of reproducing the sign reversal of the polarization observed at the CM-ICM transition[9].

YMn_2O_5 is isostructural to TbMn_2O_5 and shows the same sequence of magnetic transitions and electrical anomalies upon cooling, but the analysis of the magnetic structures is considerably simplified by the absence of magnetism on the rare earth site. Magnetic ordering appears below 45K with a CM vector, and switches to an ICM state below 23K. Similar to TbMn_2O_5 , the ferroelectric state coexists with the magnetically ordered state and at the first-order CM-ICM transition, the dielectric constant jumps to higher values whereas the spontaneous electrical polarization is reversed and decreases in amplitude to about 25% of its original value[9]. Polycrystalline YMn_2O_5 was prepared by conventional solid-state reaction in an oxygen environment. Neutron powder diffraction data were collected using the GEM diffractometer at the ISIS facility. Data were recorded on warming from 1.9K to 53K in 2K steps using a helium cryostat. A collection time of 2 hours was used at 1.9K in order to obtain high statistics data in the saturated ICM regime and 20 minutes for all other temperatures. Data analysis was performed with the program FullProF[10]. Magnetic structures were determined by using global optimization techniques (Simulated Annealing) for data collected at respectively 1.9K and 24.7K followed by final Rietveld refinements at all temperatures. During simulated annealing runs, the magnetic moments on equivalent Mn sites were constrained to be equal.

The crystal structure of YMn_2O_5 refined at 53K, space group $Pbam$, is in perfect agreement with previous studies on isostructural RMn_2O_5 , (R=Tb,Ho,Dy)[4]. As for other members of the series, there is no evidence of crystal symmetry breaking from neutron diffraction at low-temperature, due to the extremely weak atomic displacements involved. Below 45K, the data show the appearance of magnetic Bragg peaks, which can be indexed with a CM propagation vector $\mathbf{k}=(1/2,0,1/4)$ above 23K, and with an ICM $\mathbf{k}\sim(0.48,0,0.29)$ below 17K. The transition between CM and ICM states, marked by the coexistence of both magnetic phases, is of first-order type. A small discontinuous reduction of the magnetic signal is also observed on warming through the ICM-CM transition. The combined structural/magnetic Rietveld refinements, shown in figure 1 for data at 24.7K and 1.9K, are of very good qual-

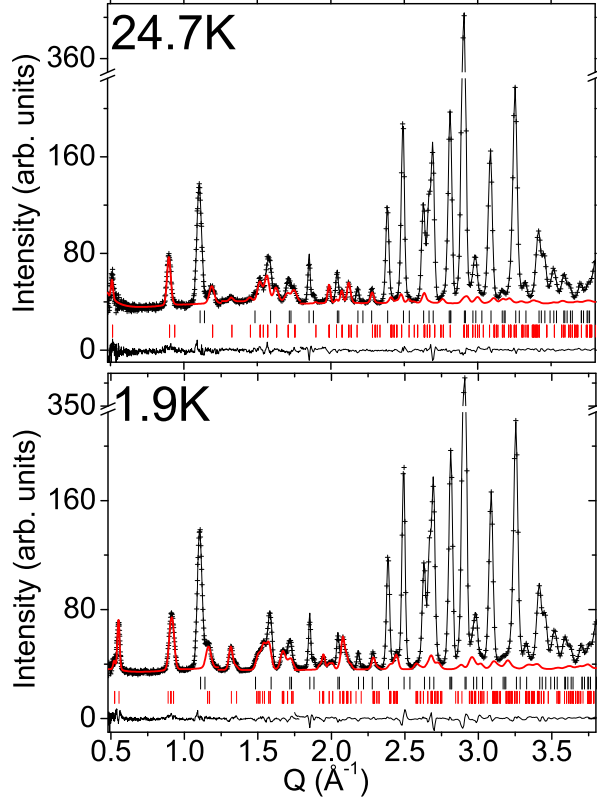


FIG. 1: Rietveld refinements at 24.7K and 1.9K. Data sets from 3 detector banks located at 18, 35 and 63.6° 2θ are merged on the same scale. The cross points and solid lines show the experimental data points and calculated profile respectively. The difference is shown on the bottom as solid lines. The upper and lower rows of markers indicate respectively the positions of the nuclear and magnetic reflections. The red line emphasizes the calculated magnetic contribution (color online).

ity, with magnetic reliability factors of 5.6% and 5.5% and χ^2 of 4.4 and 16.3 (the higher value is due to the longer collection time). The corresponding magnetic structures are displayed in figure 2, and complete lists of parameters are reported in Table I. In the CM phase, the spin arrangement, corresponding to an amplitude modulation, is similar to that found for TbMn_2O_5 [3]. The spins, directed in the ab -plane, are antiferromagnetically aligned along... Mn^{4+} ... $\text{Mn}^{3+}\text{Mn}^{3+}$... Mn^{4+} ... chains running along the a -axis. We note that, within a chain, each Mn^{3+} ion is connected to two Mn^{4+} located in layers at $z \sim 0.25$ and $(1-z)$, an important detail (see below) that is difficult to represent in the projected structure. There

are two AFM "chains" per unit cell [3]. The moments on the Mn^{3+} and Mn^{4+} sites are oriented at respective angles of $10(5)^\circ$ and $15(5)^\circ$ to the a -axis. The spins on Mn^{4+} sites at $z \sim 0.25$ and $(1-z)$, connected through the Mn^{3+} layer, are ferromagnetically (FM) aligned. A magnetic structure with constant moments, as shown in figure 2a, can be obtained when the phases are set to $\pm\pi/4$ (see below and also Table I).

The ICM magnetic structure at 1.9K also corresponds to a sinusoidal modulation of the moments (figure 2). However, this phase is a true SDW, since every amplitude value is realized on each crystallographic site. An unconstrained refinement of the initial model found by Simulated Annealing shows that magnetic moments on sites related by the glide plane operation are phased by values close to $\frac{1}{2}k_x$ ($k_x=0.479$ being the component of the propagation vector along a^*). This leads to an almost exact cancelation of the magnetic moment in one of the chains when the moments in the other chain are fully ordered. The refinement also indicates that Mn^{4+} atoms at $z \sim 0.25$ and $(1-z)$ positions, unrelated by symmetry operations of the group of the propagation vector, have phase shifts of almost $\frac{1}{2}k_z$, with $k_z=0.291$. The moments in one of the chains are at an angle of $15(4)^\circ$ to the a -axis, similar to that observed in the CM phase, while the direction of the moments in the other chain is tilted by $56(4)^\circ$. This model implies the superposition of the two irreducible representations (irreps) of the paramagnetic group, as allowed in the case of a first-order transition. The observed canting is consistent with magnetic susceptibility data[9]: the CM phase has b and c as almost equal "easy" magnetic directions. At the CM-ICM transition, b becomes a harder axis while a becomes an easier axis, again in agreement with our magnetic structure showing a rotation of half of the chains towards the b -axis. There are no anomalies in the susceptibility along c at the CM-ICM transition.

A unified description of both CM and ICM structures, consistent with the experimental data within the errors, is shown in Fig 2b. Phases on each crystallographic site within a chain have been assigned so that the moments follow a single harmonic modulation (their amplitude being related to their x fractional coordinate). The phases of the waves on adjacent chains are allowed to vary from being exactly opposite, the global phase shift between them being denoted as φ . Along c , the moments also follow a sinusoidal modulation (their amplitude being related to z'), which is the fractional coordinate ($z'=z-\frac{1}{2}$), with a phase shift ϵ with respect to the origin. We have deliberately chosen the origin of the plot to coincide with an inversion symmetry point of the ICM modulation along the a axis for $\varphi=0$

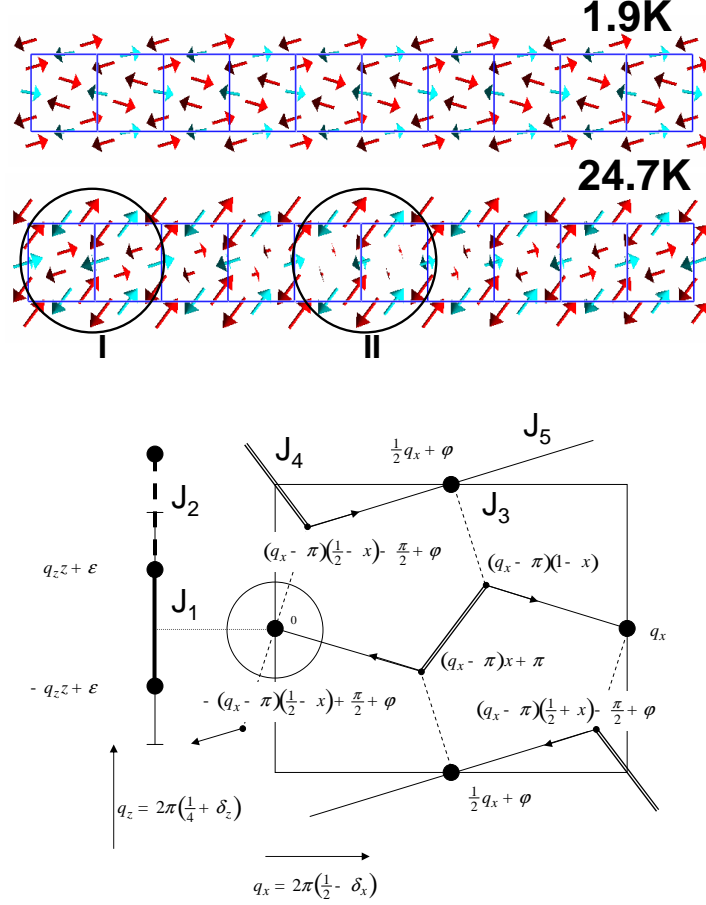


FIG. 2: (a) Magnetic structure at 24.7K (top) and 1.9K (bottom) projected in the ab -plane. Ten unit cells are displayed along a . For clarity, a single $\text{Mn}^{4+}/\text{Mn}^{3+}$ layer is shown. The light blue and red arrows represent the spins on Mn^{4+} and Mn^{3+} , respectively. For the ICM structure, region I is locally very similar to the CM phase (both chains having sizeable moments), and does not contain inversion centers. Region II could potentially contain an inversion center, and is described in more detail in Figure 2b and in the text. (b) A schematic representation of the magnetic structures of both CM and ICM phases (see text). The fragment on the left side represents a portion of the $\dots\text{Mn}^{4+}\text{-Mn}^{4+}\dots$ chains along the c -axis. The SDW phases are as shown in the labels of the Mn^{3+} sites, and are obtained for the Mn^{4+} sites by adding the values of the a - and c -axis projections. The arrows indicate the direction of the underlying *centrosymmetric* vector field that is coupled to the magnetism, and coincides with the axes of the Mn^{3+}O_5 pyramids. Magnetic exchange pathways are also indicated (color online).

and $\epsilon=0$. The CM constant-moment phase is obtained by setting the incommensurability

parameters δ_x and δ_z and the phase shift ϵ to zero, and by setting $\varphi=\pi/2$ (Figure 2b). It is clear by construction that the ICM phase is non-centrosymmetric for $\epsilon \neq 0$ and $\varphi \neq 0$. The relationship between the CM and ICM phases is also illustrated in Fig 2a. The CM phase corresponds to a local region of the ICM phase that does not contain centers of symmetry.

The value of the *net* electrical polarization along the b -axis (i.e., averaging over the oscillating components) is easily calculated based on the contribution of the symmetric inter-chain exchange interaction to the magneto-elastic coupling described in [3] and the phase factors of Fig 2b:

$$P^{ICM} = 4C\vec{S}_3 \cdot \vec{S}_4 \cos(2\pi(\frac{1}{4} + \delta_z)z') \cos(2\pi\delta_x(\frac{1}{2} - x)) \cos(\epsilon) \sin(\varphi) \quad (1)$$

where \vec{S}_3 and \vec{S}_4 are the magnetic moments on the Mn^{3+} and Mn^{4+} , respectively, and C is the magneto-elastic coupling constant. The polarization has been obtained by multiplying the magnetic terms by the b -axis component of the underlying polar field, shown with arrows in Figure 2b. From equation (1), it is clear that a non-zero value of the phase φ is required to promote a b -axis polarization. This is only possible if both irreps are involved, since for each irrep $\varphi=0$ by symmetry. In addition, the polarization direction can change depending on the value of φ .

With the help of eq. (1) and the experimental values of the phases (Table I), we can predict the value of the polarization for the ICM phase. In practice however, the error bars on the magnetic phases for an individual measurement introduce a large uncertainty on the value of the calculated polarization. To overcome this, we have fitted the weak temperature dependence of the ICM phases, to obtain constant phase differences. These yield a polarization of *opposite sign* and reduced by approximately a factor of 5 with respect to the CM phase, in close agreement with the experimental values determined by Kagomiya *et al.* [9]. The temperature dependence of the spontaneous polarization has been calculated, and is shown in Figure 3 to be in good agreement with the experimental curve by Kagomiya and co-workers [9].

Although $\varphi \neq 0$ is clearly allowed by symmetry in our case, and as we have shown this can lead to a spontaneous polarization of either sign in the ICM phase, it is presently unclear to us how a non-zero value can be energetically favorable. In fact, in the simple isotropic exchange model, the inter-chain energy can be written as:

$$E_3^{ICM} = -4J_3\vec{S}_3 \cdot \vec{S}_4 \cos(2\pi(\frac{1}{4} + \delta_z)z') \sin(2\pi\delta_x(\frac{1}{2} - x)) \cos(\epsilon) \cos(\varphi) \quad (2)$$

which is even in φ . It is noteworthy however, that E_3^{ICM} is linear in δ_x for small δ_x , suggesting a natural mechanism to stabilize the incommensurability along the a axis.

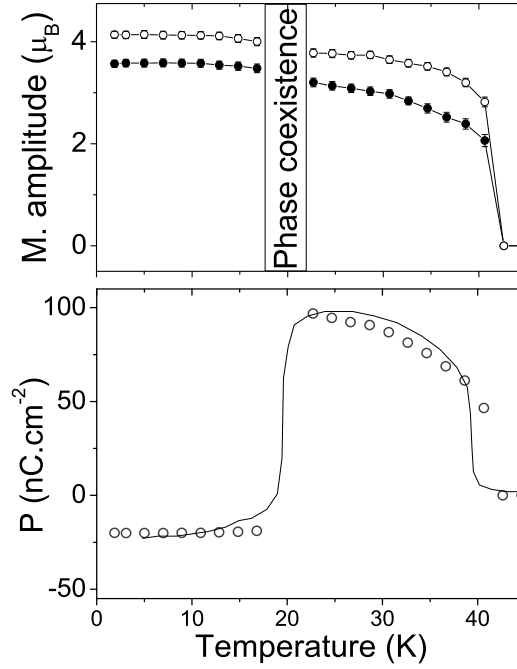


FIG. 3: (a) Refined values of the magnetic wave amplitudes on Mn^{3+} (open symbols) and Mn^{4+} (filled symbols) as a function of temperature. The *average* moment on each site is $\frac{1}{\sqrt{2}}$ of the wave amplitude. (b) **Symbols:** electrical polarization of YMn_2O_5 , as calculated from eq. (1). **Solid line:** Experimental values of the electrical polarization, extracted from Kagomiya *et al.* [9]. The calculated polarization has been scaled by a single constant to account for the unknown magneto-elastic coupling parameter.

In summary, we have developed a model to explain the presence of ferroelectricity in the CM and ICM phases of YMn_2O_5 *without* the need to invoke non-collinearity and/or chirality as essential features. We show that ferroelectricity is compatible with an acentric SDW, which the literature reports as the most probable magnetic structure for this class

TABLE I: Magnetic parameters obtained from Rietveld refinements of the 1.9K and 24.7K data.

Atom	Position	24.7K			1.9K		
		$M_x(\mu_B)$	$M_y(\mu_B)$	Phase(rad)	$M_x(\mu_B)$	$M_y(\mu_B)$	Phase(rad)
Mn ⁴⁺	(0 0.5 0.255)	3.092(9)	-0.5(2)	$\frac{\pi}{4}$	-3.46(8)	-0.9(1)	-0.459
Mn ⁴⁺	(0.5 0 0.255)	-3.092(9)	-0.5(2)	$\frac{\pi}{4}$	-1.9(2)	-3.0(1)	4.15(69)
Mn ⁴⁺	(0 0.5 0.745)	3.092(9)	-0.5(2)	$\frac{\pi}{4}$	-3.46(8)	-0.9(1)	0.459
Mn ⁴⁺	(0.5 0 0.745)	-3.092(9)	-0.5(2)	$\frac{\pi}{4}$	-1.9(2)	-3.0(1)	5.09(69)
Mn ³⁺	(0.412 0.351 0.5)	-3.63(9)	-1.0(2)	$\frac{\pi}{4}$	-4.02(8)	-1.0(2)	2.83(44)
Mn ³⁺	(0.588 0.649 0.5)	3.63(9)	1.0(2)	$\frac{\pi}{4}$	-4.02(8)	-1.0(2)	-0.31(44)
Mn ³⁺	(0.088 0.851 0.5)	3.63(9)	1.0(2)	$\frac{\pi}{4}$	-2.5(2)	-3.3(2)	1.44(81)
Mn ³⁺	(0.912 0.149 0.5)	3.63(9)	1.0(2)	$\frac{\pi}{4}$	-2.5(2)	-3.3(2)	1.44(81)

of materials[11, 12]. We have determined the high-temperature commensurate and low-temperature incommensurate magnetic structures of YMn_2O_5 based on neutron diffraction data. The calculated electrical polarization based on our model and a simple magneto-elastic coupling was found to be in good agreement with the experimental values at all temperatures, including a previously unexplained sign reversal at the CM-ICM transition. We would like to acknowledge helpful discussions with Daniel Khomskii, Maxim Mostovoy and Joseph Betouras.

-
- [1] T. Kimura, T. Goto, H. Shintani, K. Ishizaka, T. Arima, and Y. Tokura, Nature (London) **426**, 55 (2003).
 - [2] N. Hur, S. Park, P.A.Sharma, J. Ahn, S. Guha, and S.-W. Cheong, Nature **429**, 392 (2004).
 - [3] L. C. Chapon, G. R. Blake, M. J. Gutmann, S. Park, N. Hur, P. G. Radaelli, and S.-W. Cheong, Physical Review Letters **93**, 177402 (2004).
 - [4] G. R. Blake, L. C. Chapon, P. G. Radaelli, S. Park, N. Hur, S.-W. Cheong, and J. Rodriguez-Carvajal, Physical Review B **71**, 214402 (2005).
 - [5] M. Kenzelmann, A. B. Harris, S. Jonas, C. Broholm, J. Schefer, S. B. Kim, C. L. Zhang, S.-W. Cheong, O. P. Vajk, and J. W. Lynn, Physical Review Letters **95**, 087206 (2005).

- [6] W. Ratcliff, II, V. Kiryukhin, M. Kenzelmann, S.-H. Lee, R. Erwin, J. Schefer, N. Hur, S. Park, and S.-W. Cheong, Physical Review B **72**, 060407(R) (2005).
- [7] I. A. Sergienko and E. Dagotto, cond-mat/0508075 (2005).
- [8] G. Lawes, A. B. Harris, T. Kimura, N. Rogado, R. J. Cava, A. Aharony, O. Entin-Wohlman, T. Yildirim, M. Kenzelmann, C. Broholm, et al., Physical Review Letters **95**, 087205 (2005).
- [9] I. Kagomiya, S. Matsumoto, K. Kohn, Y. Fukuda, T. Shoubu, H. Kimura, Y. Noda, and N. Ikeda, Ferroelectrics **286**, 167 (2003).
- [10] J. Rodriguez-Carvajal, Physica B **192**, 55 (1993).
- [11] C. Wilkinson, F. Sinclair, P. Gardner, J. B. Forsyth, and B. M. R. Wanklyn, J. Phys. C-Solid St. Phys. **14**, 1671 (1981).
- [12] P. P. Gardner, C. Wilkinson, J. B. Forsyth, and B. M. Wanklyn, J. Phys. C: Solid State Phys. **21**, 5653 (1988).